Electronic Supplementary Information

Highly stable poly-nitro components achieved through supramolecular encapsulation

Authors: Jichuan Zhang[1], Jinhao Zhang[2], Jatinder Singh[1], Wanbao Wu[3], Richard J. Staples[4], Jiaheng Zhang[2],* and Jean'ne M. Shreeve[1]*

Affiliations:

[1]Department of Chemistry, University of Idaho, Moscow, Idaho 83844-2343, United States

[2]Sauvage Laboratory for Smart Materials, Harbin Institute of Technology, Shenzhen 518055, China

[3]School of Petrochemical Engineering, Changzhou University, Changzhou 213000, China

[4]Department of Chemistry, Michigan State University, East Lansing, Michigan 48824, United States

*Correspondence to: Jean'ne M. Shreeve (jshreeve@uidaho.edu)

Page

EXPERIMENTAL SECTION

Caution! The cocrystals in this work are energetic materials that could potentially explode under certain conditions (e.g., impact, friction, or electric discharge). Appropriate safety precautions, such as the use of shields in a fume hood and personal protection equipment (safety glasses, face shields, ear plugs, as well as gloves) should be taken at all times when handling these materials.

General. Melamine was purchased from Alfa Aesar in analytical grade and was used as supplied. ^{1}H NMR and ^{13}C NMR spectra were recorded on a 300 MHz (Bruker AVANCE 300) nuclear magnetic resonance spectrometer. Chemical shifts for ^{1}H, ^{13}C and ^{15}N NMR spectra are given with respect to external $(CH_3)_4Si$ (^{1}H and ^{13}C). [D_6]DMSO was used as a locking solvent unless otherwise stated. IR spectra were recorded using KBr pellets with a FT-IR spectrometer (Thermo Nicolet AVATAR 370). Density was determined at room temperature by employing a Micromeritics AccuPyc II 1340 gas pycnometer. Decomposition temperatures (onset) were recorded using a dry nitrogen gas purge and a heating rate of 5 °C min^{-1} on a differential scanning calorimeter (DSC, TA Instruments Q2000). Elemental analyses (C, H, N) were performed with a Vario Micro cubeElementar Analyzer. Impact and friction sensitivity measurements were made using a standard BAM Fallhammer and a BAM friction tester.

Supplementary section 1: Preparation of supramolecules

The preparation of MA@DN, MA@NF, and MA@TNP are similar. Ammonium dinitramide (ADN, 0.124 g, 1 mmol)/ hydrazinium nitroform (HA-NF, 0.183 g, 1 mmol)/ 3,4,5-trinitropyrazolate (TNP, 0.203 g, 1 mmol) was added to the preheated H_2O (30 mL, 60 ℃), which contains melamine (0.252 g, 2 mmol). After stirring for ~30 min, the mixture was filtered, and the filtrate was allowed to set about 3-5 days, and yellow or colorless crystals precipitated. The crystals were filtered, washed by a small amount of water and dried.

The preparations of TATOT@DN, TATOT@NF, and TATOT@TNP are similar. Ammonium dinitramide (ADN, 0.248g, 1 mmol)/ hydrazinium nitroform (HA-NF, 0.183 g, 1 mmol)/ 3,4,5-trinitro-pyrazolate (TNP, 0.203 g, 1 mmol) was added to 30 mL H_2O. The solution was heated at 60 ℃. 3,6,7-Triamino-7H-[1,2,4]triazolo[5,1-c][1,2,4]-triazole hydrochloride (TATOT·HCl, 0.1615g, 1 mmol) and 3,6,7-triamino-7H-[1,2,4]triazolo[5,1-c][1,2,4]-triazole (TATOT, 0.126g, 1 mmol) were added to the above system. After 30 minutes stirring at 60 ℃, the mixture was cooled to room temperature, and filtered. After 3 days, colorless plate crystals were obtained. They were filtered, washed with a little H_2O and dried for characterization.

MA@DN: Colorless plate crystal, yield: 72% (based on MA). ^{1}H NMR (300 MHz, d_6-DMSO) δ 6.92 (s, 3NH_2, 6H), 4.70 (s, $^{+}$NH, 1H). ^{13}C NMR (75 MHz, d_6-DMSO) δ 163.23. IR (KBr pellet): $\tilde{\nu}$ 3444, 3401, 3171, 2963, 1655, 1535, 1469, 1361, 1185, 1016, 819, 785, 739, 670, 567, 523 cm^{-1}. Elemental analysis calcd. (%) for $C_6H_{13}N_{15}O_4$ (359.27): C (20.06), H (3.65), N (58.48); found: C (20.26), H (3.64), N (59.23).

MA@NF: Yellow chunk crystal, yield: 69% (based on MA). ^{1}H NMR (300 MHz, d_6-DMSO) δ 6.90 (s, 3NH_2, 6H), 5.36 (s, $^{+}$NH, 1H). ^{13}C NMR (75 MHz, d_6-DMSO) δ 160.99, 119.86. IR (KBr pellet): $\tilde{\nu}$ 3581, 3449, 3405, 1671, 1614, 1524, 1461, 1416, 1278, 1167, 1095, 1017, 820, 785, 729, 580,523 cm^{-1}. Elemental analysis calcd. (%) for $C_7H_{13}N_{15}O_6$ (403.28): C (20.85), H (3.25), N (52.10); found: C (20.13), H (3.43), N (51.54).

MA@TNP: Yellow plate-shaped crystal, yield: 75% (based on MA). ^{1}H NMR (300 MHz, d_6-DMSO) δ 7.09

(s, 3NH_2, 6H), 4.91 (s, $^+$NH, 1H). ^{13}C NMR (75 MHz, d_6-DMSO) δ 159.66, 146.83, 121.94. IR (KBr pellet): ṽ 3644, 3459, 3416, 3357, 2934, 1669, 1550, 1451, 1362, 1324, 1172, 1132, 1010, 847, 816, 784, 725, 679, 592, 527, 405 cm^{-1}. Elemental analysis calcd. (%) for $C_9H_{13}N_{17}O_6$ (455.32): C (23.74), H (2.88), N (52.30); found: C (23.66), H (2.93), N (52.29).

TATOT@DN: Yellow block crystal, yield: 70% (based on TATOT). ^{1}H NMR (300 MHz, d_6-DMSO) δ 8.13 (s, NH_2, 2H), 6.80 (s, NH_2, 2H), 5.68 (s, NNH_2, 2H). ^{13}C NMR (75 MHz, d_6-DMSO) δ 159.441, 148.25, 142.35. IR (KBr pellet): ṽ 3433, 3345, 3244, 3175, 2698, 1691, 1652, 1562, 1511, 1429, 1339, 1250, 1181, 1097, 1008, 875, 757, 725, 621, 592, 466 cm^{-1}. Elemental analysis calcd. (%) for $C_9H_{13}N_{17}O_6$ (455.32): C (23.74), H (2.88), N (52.30); found: C (23.66), H (2.93), N (52.29).

TATOT@NF (5): Yellow block crystal, yield: 76% (based on TATOT). ^{1}H NMR (300 MHz, d_6-DMSO) δ 6.83 (s, NH_2, 2H), 5.67 (s, NH_2, 2H), 4.49 (s, NNH_2, 2H). ^{13}C NMR (75 MHz, d_6-DMSO) δ 159.34, 148.10, 142.20, 117.46. IR (KBr pellet): ṽ 3407, 3359, 3239, 3170, 1699, 1649, 1526, 1470, 1399, 11086, 1037, 976, 907, 784, 729, 600, 500 cm^{-1}. Elemental analysis calcd. (%) for $C_9H_{13}N_{17}O_6$ (455.32): C (23.74), H (2.88), N (52.30); found: C (23.66), H (2.93), N (52.29).

TATOT@TNP (6): Yellow needle-shaped crystal, yield: 78% (based on TATOT). ^{1}H NMR (300 MHz, d_6-DMSO) δ 7.09 (s, 3NH_2, 6H), 4.91 (s, $^+$NH, 1H). ^{13}C NMR (75 MHz, d_6-DMSO) δ 159.29, 148.15, 142.24, 121.97. IR (KBr pellet): ṽ 3430, 3344, 3249, 3174, 1679, 1512, 1451, 1417, 1357, 1320, 1291, 1127, 1083, 901, 848, 806, 760, 706, 617, 545, 445 cm^{-1}. Elemental analysis calcd. (%) for $C_9H_{13}N_{17}O_6$ (455.32): C (23.74), H (2.88), N (52.30); found: C (23.66), H (2.93), N (52.29).

Supplementary section 2: Single crystal data information

Crystal MA@DN, a colorless plate crystal with dimensions 0.47×0.19×0.02 mm^3 was mounted on a nylon loop with Paratone oil. Data were collected using a Bruker APEX-II CCD diffractometer equipped with an Oxford Cryosystems low-temperature device, operating at T = 172.99 K. Crystal MA@NF, a yellow chunk crystal with dimensions 0.31×0.20×0.05 mm^3 was mounted on a nylon loop with Paratone oil. Data were collected using a Bruker APEX-II CCD diffractometer equipped with an Oxford Cryosystems low-temperature device, operating at T = 173(1) K. Crystal MA@TNP, a yellow plate-shaped crystal with dimensions 0.38×0.10×0.03 mm^3 was mounted on a nylon loop with Paratone oil. Data were collected using a Bruker APEX-II CCD diffractometer equipped with an Oxford Cryosystems low-temperature device, operating at T = 100.00(10) K. Crystal TATOT@DN, a yellow block crystal with dimensions 0.18×0.14×0.12 mm^3 was mounted on a nylon loop with Paratone oil. Data were collected using a Bruker APEX-II CCD diffractometer equipped with an Oxford Cryosystems low-temperature device, operating at T = 99.99(10) K. Crystal TATOT@NF, a yellow block crystal with dimensions 0.21×0.05×0.04 mm^3 was mounted on a nylon loop with Paratone oil. Data were collected using a Bruker APEX-II CCD diffractometer equipped with an Oxford Cryosystems low-temperature device, operating at T = 100.01(15) K. Crystal TATOT@TNP, a yellow plate-shaped crystal with dimensions 0.30×0.03×0.01 mm^3 was mounted on a nylon loop with paratone oil. Data were collected using a Bruker APEX-II CCD diffractometer equipped with an Oxford Cryosystems low-temperature device, operating at T = 99.97(12) K.

Table S1. Crystallographic data and structure refinement parameters of MA@DN, MA@NF, and MA@TNP.

Crystal	MA@DN	MA@NF	MA@TNP
CCDC	1992828	1992827	2298706
Empirical formula	$C_6H_{17}N_{15}O_6$	$C_7H_{15}N_{15}O_7$	$C_9H_{17}N_{17}O_8$
Formula mass	395.34	421.34	491.39
Crystal system	triclinic	triclinic	triclinic
Space group	$P\bar{1}$	$P\bar{1}$	$P\bar{1}$
Z	1	2	2
a (Å)	3.5829(2)	7.18570(10)	7.6620(3)
b (Å)	9.4348(4)	9.6805(2)	8.8898(3)
c (Å)	12.7509(6)	12.5342(2)	15.2446(6)
α (°)	111.044(2)	107.4430(10)	88.151(3)
β (°)	91.470(3)	93.9270(10)	75.617(3)
γ (°)	100.508(3)	98.7430(10)	78.738(3)
Volume (Å^3)	393.58(3)	816.10(2)	986.31(6)
D_{calc} (g cm^{-3})	1.668	1.715	1.655
Temperature (K)	172.99	173(1)	100.00(10)
F(000)	206.0	436.0	508.0
h, k, l	4, 11, 15	8, 11, 15	9, 11, 19
μ (cm^{-1})	1.263	1.314	1.256
R_1 [I > 2σ(I)]	0.0.347	0.0343	0.0325
Completeness to theta full (%)	98	98	99.8
wR_2 (all data)	0.0934	0.0987	0.0897
S on $F2$	1.065	1.035	1.063

Table S2. Crystallographic data and structure refinement parameters of **TATOT@DN, TATOT@NF**, and **TATOT@TNP**.

Crystal	TATOT@DN	TATOT@NF	TATOT@TNP
CCDC	2298707	2298704	2298705
Empirical formula	$C_6H_{13}N_{19}O_4$	$C_7H_{13}N_{19}O_6$	$C_9H_{17}N_{21}O_8$
Formula mass	415.35	459.36	547.43
Crystal system	triclinic	triclinic	monoclinic
Space group	$P\bar{1}$	$P\bar{1}$	$I2/a$
Z	2	2	8
a (Å)	7.67260(10)	7.81700(11)	28.7396(7)
b (Å)	11.0852(2)	10.91472(18)	3.67148(8
c (Å)	11.3570(2)	12.38082(16)	40.1450(8)
α (°)	117.502(2)	64.1208(14)	90
β (°)	93.621(2)	88.5853(11)	99.639(2)
γ (°)	107.842(2)	70.3756(14)	90
Volume (Å^3)	791.26(3)	885.89(3)	4176.17(16)
D_{calc} (g cm^{-3})	1.743	1.722	1.741
Temperature (K)	99.99(10)	100.01(15)	99.97(12)
F(000)	428.0	472.0	2256.0

h, k, l	9, 14, 14	9, 13, 15	34, 4, 51
μ (cm-1)	1.277	1.298	1.319
Formula Weight			
R_1 [I > 2σ(I)]	0.0349	0.0442	0.0570
Completeness to theta full (%)	100	100	98.6
wR_2 (all data)	0.0936	0.1224	0.1572
S on *F2*	1.049	1.062	1.066

Supplementary section 3: Lengths of hydrogen bonds in selected structures of DN, NF, and TNP

Table S3. Lengths of hydrogen bonds for DN series.

	MA@DN	**TATOT@DN**	**TATB-DN**[1]
N-H···O	2.132 Å	2.093 Å	2.041 Å
	2.173 Å	2.180 Å	2.156 Å
	2.224 Å	2.204 Å	2.212 Å
	2.225 Å	2.267 Å	2.260 Å
	2.226 Å	2.272 Å	2.328 Å
	2.501 Å	2.394 Å	2.426 Å
		2.402 Å	2.500 Å
		2.445 Å	
N-H···N		2.469 Å	

Table S4. Lengths of hydrogen bonds for NF series.

	MA@NF	**MA-TATOT@NF**[2]	**TATOT@NF**	**MA-NF**[3]
N-H···O	2.154 Å	2.150 Å	2.130 Å	2.052
	2.208 Å	2.226 Å	2.192 Å	2.071
	2.216 Å	2.233 Å	2.207 Å	2.078
	2.236 Å	2.236 Å	2.228 Å	2.148
	2.238 Å	2.281 Å	2.259 Å	2.205
	2.276 Å	2.298 Å	2.287 Å	2.274
	2.362 Å	2.309 Å	2.316 Å	2.290
	2.472 Å	2.330 Å	2.526 Å	
	2.536 Å	2.362 Å		
		2.387 Å		
		2.388 Å		

Table S5. Lengths of hydrogen bonds for TNP series.

	MA@TNP	**TATOT@TNP**	**TATOT-TNP**[4]
N-H···O	2.029 Å	2.365 Å	2.228
	2.163 Å	2.371 Å	2.336
	2.199 Å	2.461 Å	
	2.461 Å	2.479 Å	
	2.472 Å	2.515 Å	
		2.535 Å	
N-H···N	1.968	2.209	2.014
	2.209	2.269	2.213

Supplementary section 4: The distribution of hydrogen bonds around anion for selected DN, NF, and TNP structures

Hydrogen bond frame structures of anions for DN, NF, and TNP series is shown in Figure S1, S2, and S3, respectively. It can be seen that in the supramolecular structure, not only the anions are tightly fixed to the surrounding cations or molecules, but also the cations or molecules can further stabilize their structure through hydrogen bonding. Therefore, DN, NF and TNP series with supramolecular structure have higher stability than their salts. Meanwhile, DN, NF and TNP series supramolecules form different network structures through hydrogen bonding. Among them, the MA series supramolecules form two-dimensional planar structures, while the TATOT series supramolecules form three-dimensional frame structures.

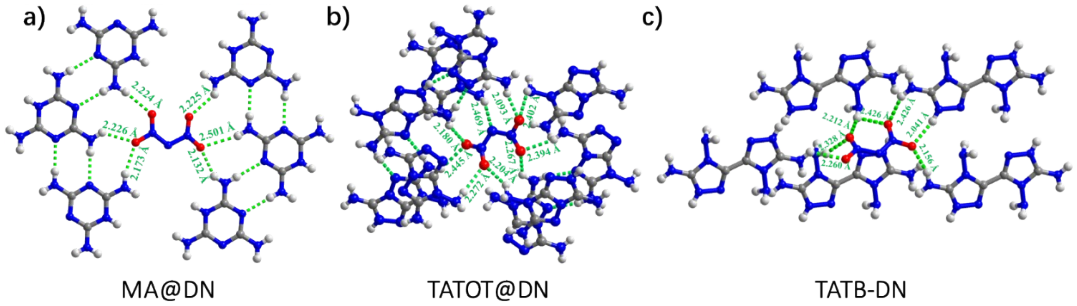

Figure S1. Hydrogen bond frame structure of anion for DN series.

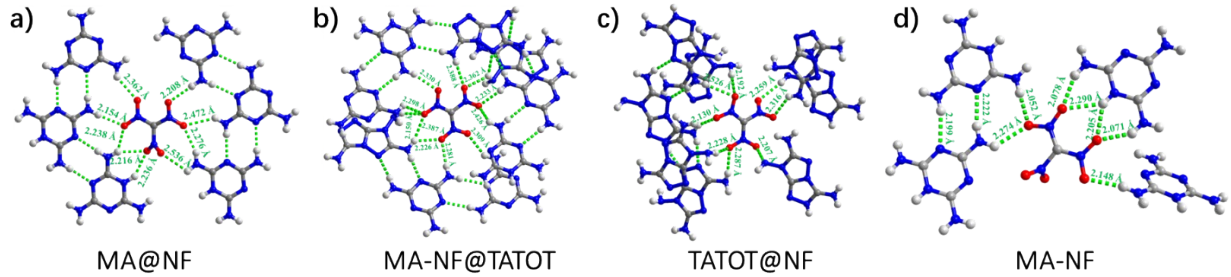

Figure S2. Hydrogen bond framework structure of anion for NF series.

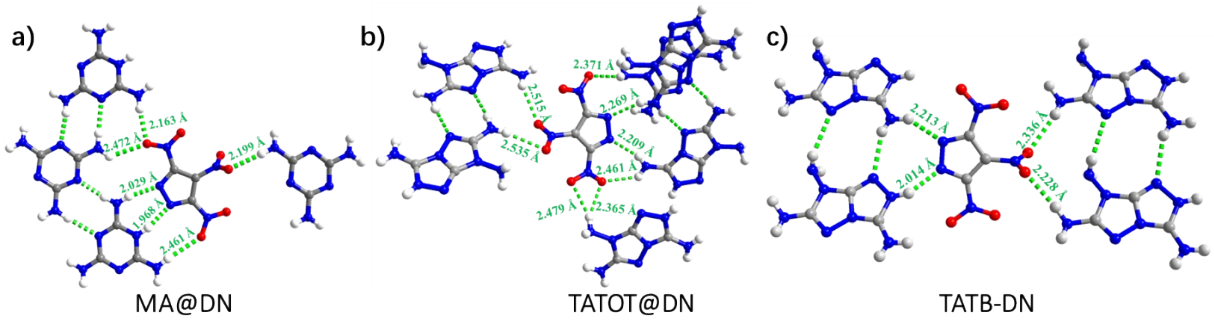

Figure S3. Hydrogen bond frame structure of anion for TNP series.

Supplementary section 5: Differential Scanning Calorimetry (DSC) and Thermogravimetric analysis (TGA) of selected samples

DSC determinations show that the crystal H_2O in MA@DN, MA@NF, MA@TNP and TATOT@TNP sublime before decomposition, and the decomposition temperatures and thermal behaviors of hydrated samples are almost the same as anhydrous samples, except for the disappearance of the endothermic H_2O peak which suggests that the removal of lattice water molecule doesn't change the supramolecule structure. Their onset decomposition temperatures are obtained from the tangent line, as shown in Figure S4-S9.

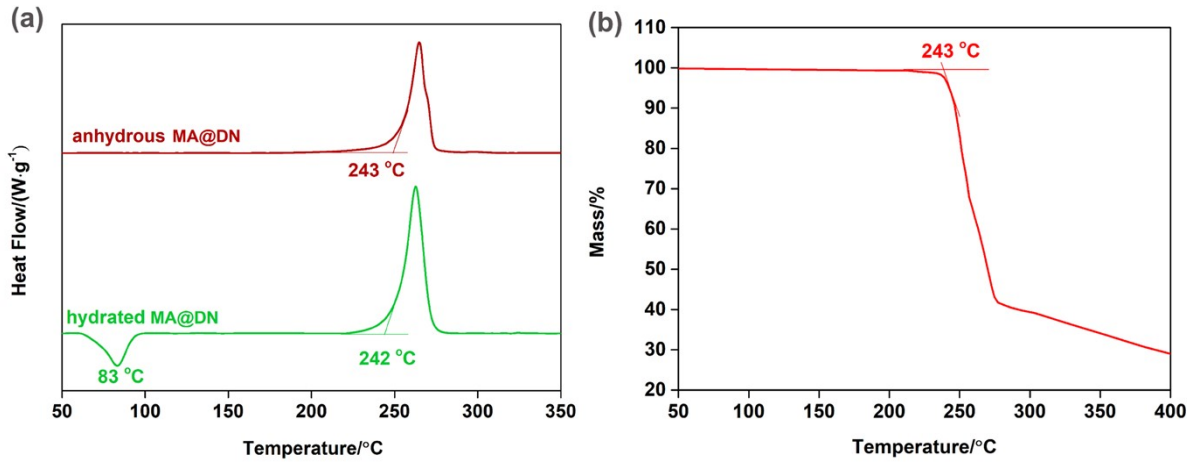

Figure S4. DSC and TGA thermal behaviors of MA@DN; a) DSC of MA@DN and anhydrous MA@DN, b) TGA of anhydrous MA@DN (5 °C min^{-1} under N_2 atmosphere)

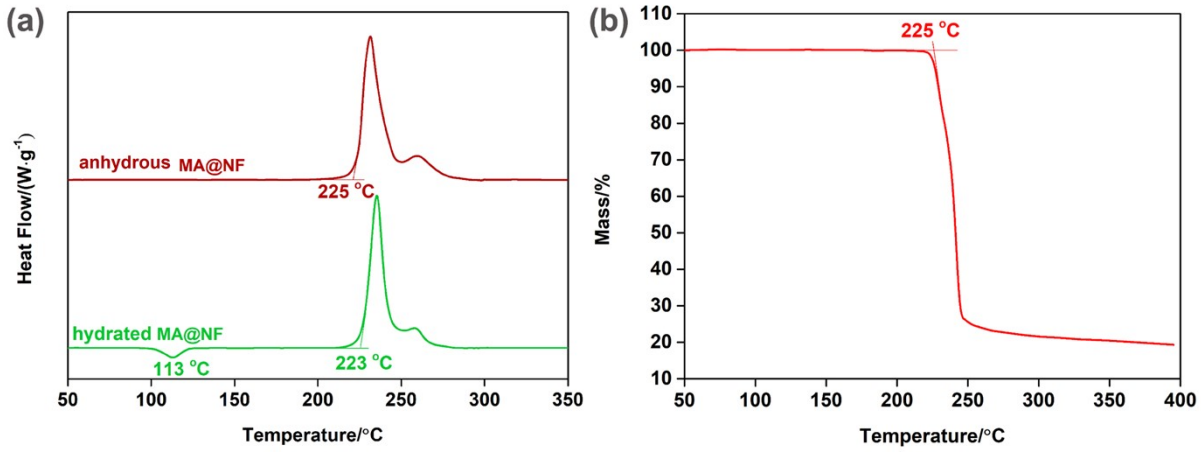

Figure S5. DSC and TGA thermal behaviors of MA@NF; a) DSC of MA@NF and anhydrous MA@NF, b) TGA of anhydrous MA@NF (5 °C min^{-1} under N_2 atmosphere)

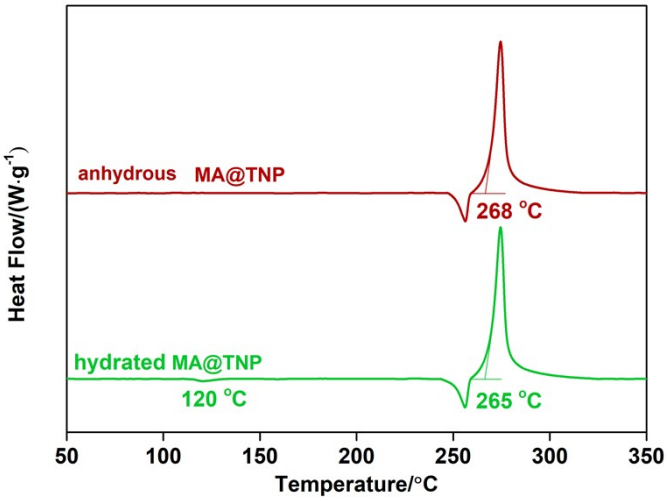

Figure S6. DSC thermal behaviors of MA@TNP and anhydrous MA@TNP (5 °C min^{-1} under N_2 atmosphere)

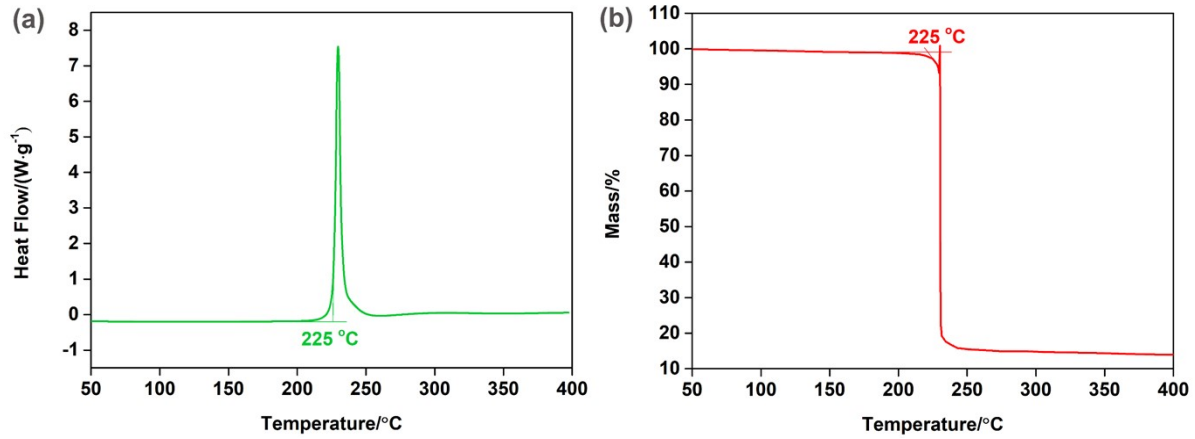

Figure S7. DSC and TGA thermal behaviors of TATOT@DN (5 ℃ min^{-1} under N_2 atmosphere)

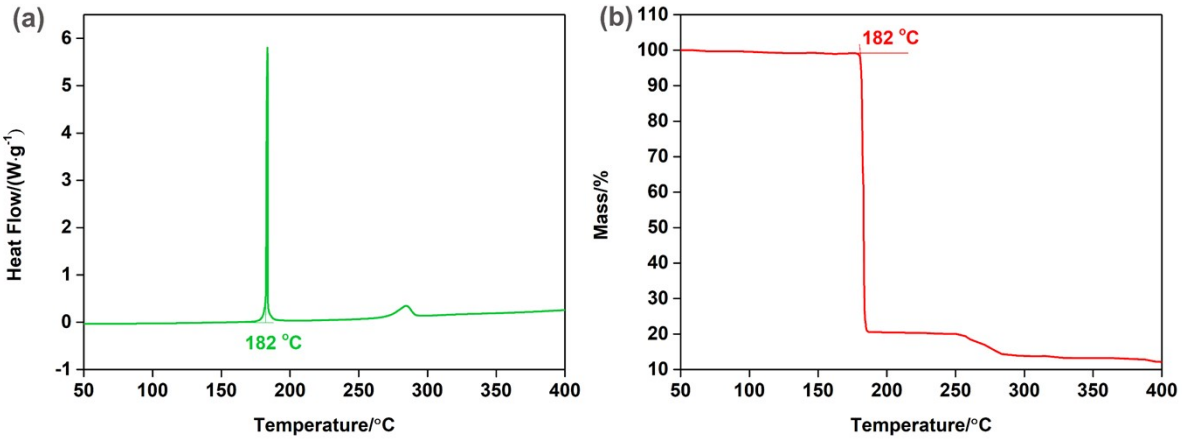

Figure S8. DSC and TGA thermal behaviors of TATOT@NF (5 ℃ min^{-1} under N_2 atmosphere)

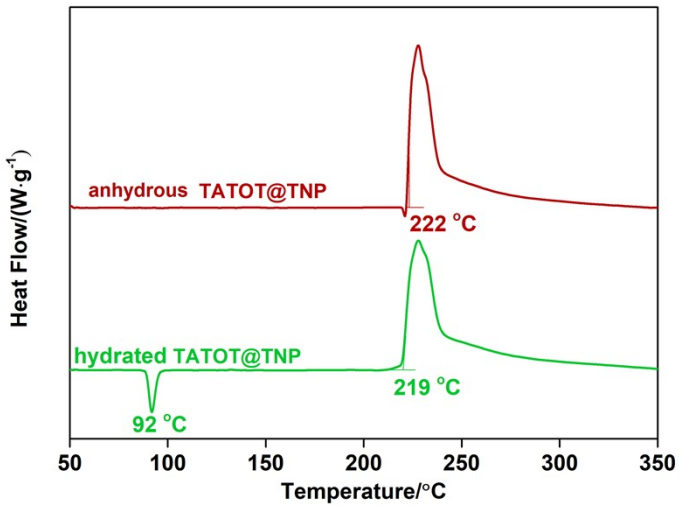

Figure S9. DSC thermal behavior of TATOT@TNP and anhydrous TATOT@TNP (5 ℃ min^{-1} under N_2 atmosphere)

Supplementary section 6: NCI and ESP calculations

The geometries of the unit cells were optimized at the B3LYP/6-31+G** using Gaussian 03 (Revision D.01) suite of scripts[5-7]. The noncovalent interaction (NCI) index demonstrates the detailed nature of the weak-to-strong stabilizing/destabilizing interactions within and between molecules and possesses paramount

importance in governing the physicochemical properties of energetic materials. The NCI index classifies the attractive or repulsive interactions according to the sign of the second-density Hessian eigenvalue (I_2) and electron density (r) that is sin (I_2)r. The 2D plots between the reduced density gradient (RDG) and sin(I_2)r and ESP for the studied DN, NF, and TNP series of cocrystals are shown in Figure S10-S12. The NCI and ESP plots were drawn using two softwares: Multiwfn and VMD.[8-9]

The calculations of NCI and ESP based on the optimized anhydrous structures results show that among the compounds of DN, NF, and TNP anion series, the supramolecule formed with MA has the strongest weak interaction (hydrogen bond) and the lowest anion maximum value (for DN series: MA@DN(41.14 kcal·mol^{-1}) < TATOT@DN(41.78 kcal·mol^{-1}) < TABT-DN (44.79 kcal·mol^{-1}); for NF series: MA@NF(43.39 kcal·mol^{-1}) < MA-NF@TATOT(47.98 kcal·mol^{-1}) < TATOT@DN(49.87 kcal·mol^{-1}) < MA-NF(50.54 kcal mol^{-1}); for TNP series: MA@TNP(48.08 kcal·mol^{-1}) < TATOT@TNP(48.32 kcal·mol^{-1}) < TABT-DN(49.29 kcal·mol^{-1})), followed by the supramolecule formed with TATOT, and finally the salt, which is also relative to their thermal stability.

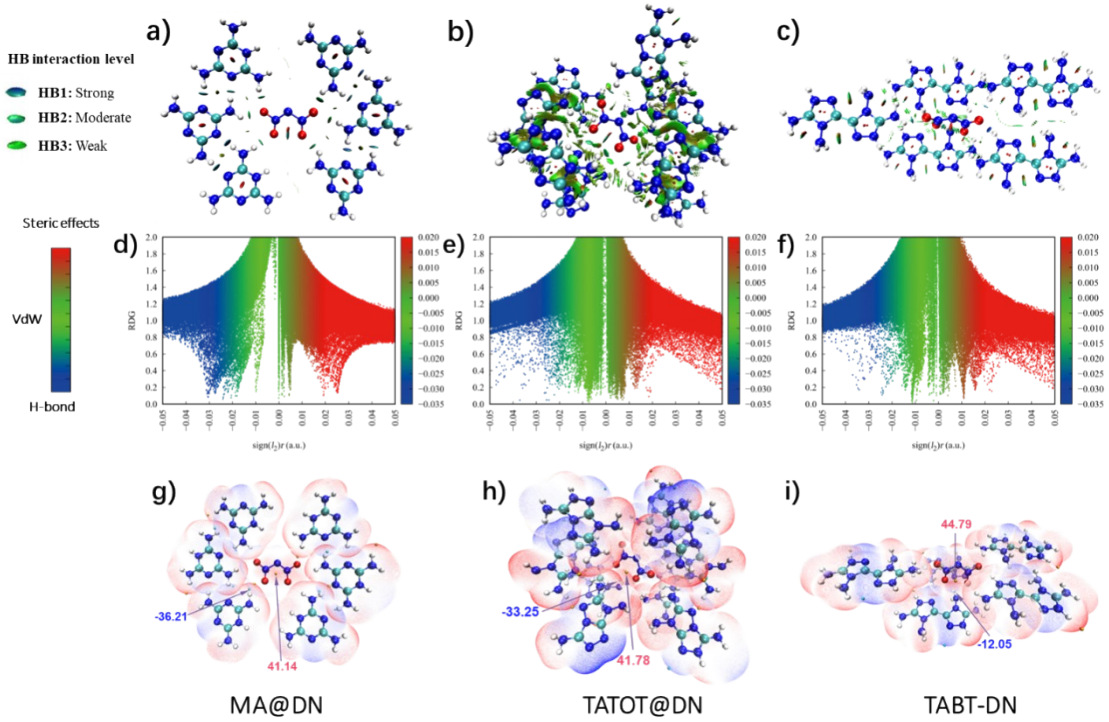

Figure S10. NCI (Noncovalent interaction) and ESP (Electrostatic potential) calculations for MA@DN, TATB-DN, and TATOT@DN.

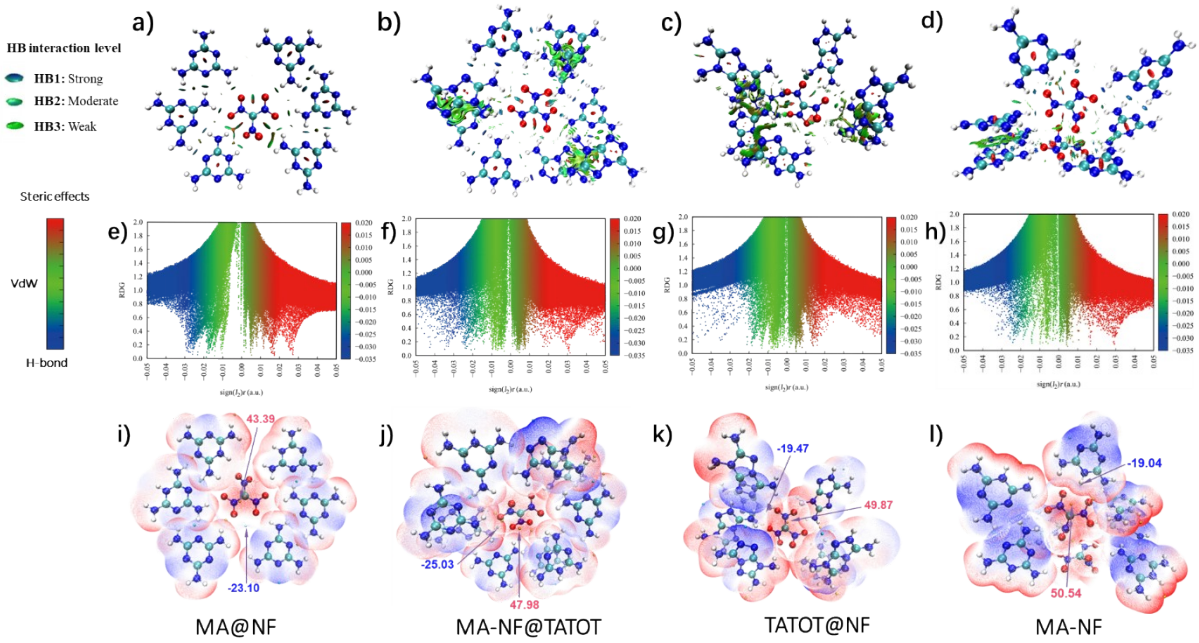

Figure S11. NCI (Noncovalent interaction) and ESP (Electrostatic potential) calculations for MA@NF, MA-NF@TATOT, TATOT@NF, and MA-NF

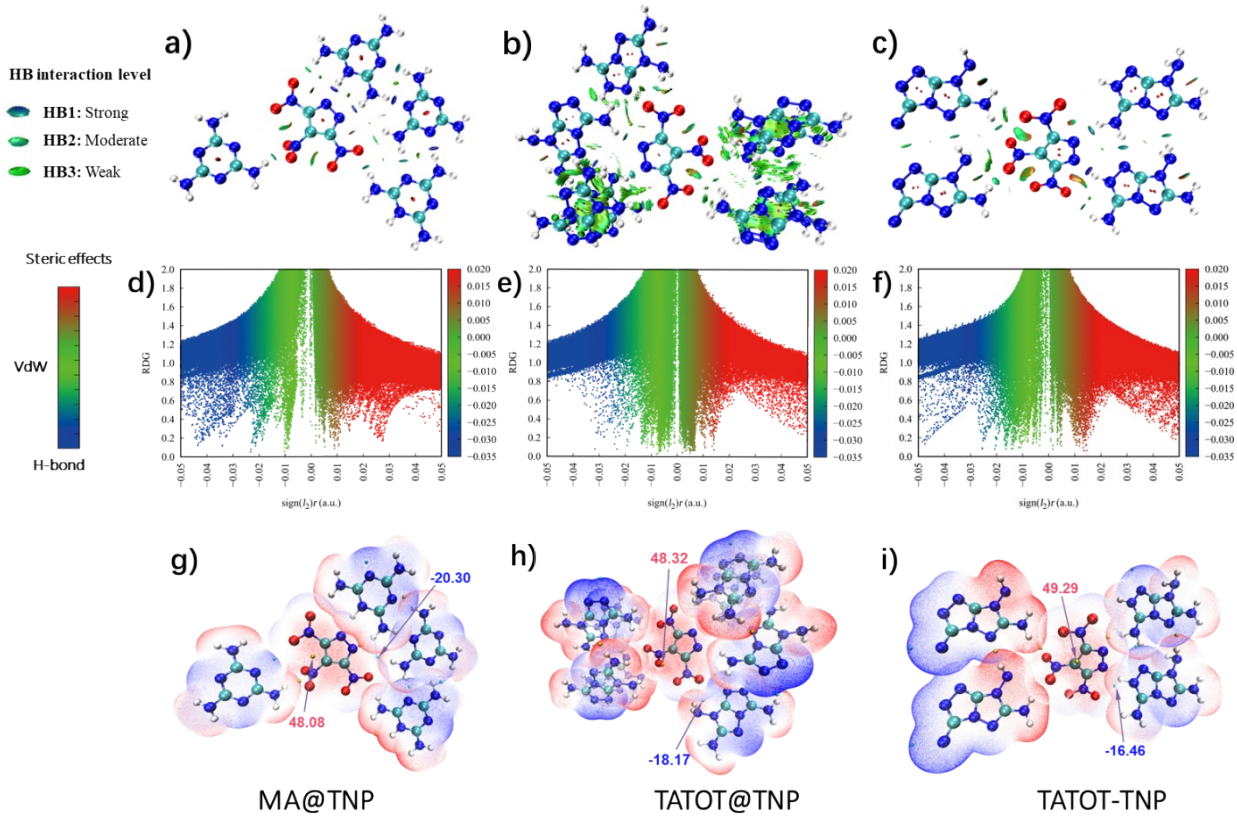

Figure S12. NCI (Noncovalent interaction) and ESP (Electrostatic potential) calculations for MA@TNP, TATOT@TNP, and TATOT-TNP

Table S6. Maximum and Minimum ESP values for selected structures for DN, NF and TNP.

Structure	Maximum values of anion	Minimum values of anion
MA@DN	41.14	-36.21
TATOT@DN	41.78	-33.25
TATB-DN	44.79	-12.05
MA@NF	43.39	-23.10
MA-TATOT@NF	47.98	-25.03
TATOT@NF	49.87	-19.47
MA-NF	50.54	-19.04
MA@TNP	48.08	-20.30
TATOT@TNP	48.32	-18.17
TATOT-TNP	49.29	-16.46

Supplementary section 7: Hirshfeld surfaces

To further investigate that the supramolecules formed by MA or TATOT in this work have better thermal stability than the energetic compounds of the same type of poly-nitroionic or supramolecular compounds, 2D fingerprints and associated Hirshfeld surfaces of the same type of poly-nitroionic or supramolecular compounds are used to determine the intermolecular interactions[10-11]. The 2D-fingerprint plots in crystal stacking for salts or supramolecular compounds of NF^- anion and TNP^- anion as well as their associated Hirshfeld surfaces are shown in Figure S13-S14, respectively. The involved software for Hirshfield surface (2D fingerprint plots) is CrystalExplorer[12].

For poly-nitro compounds, the higher the proportion of N···O and O···O interactions in the whole weak interaction, the lower the stability. 2D fingerprint calculations based on Hirshfeld surfaces of NF and TNP series disclose that the sum of N···O and O···O interactions of MA@NF=MA-NF@TATOT<TATOT@NF<MA-NF are 3.7, 3.7, 6.6, and 13.5%, MA@TNP<TATOT@TNP<TATOT-TNP are 6.4, 88.3 and 15.7%, respectively, which supports the order of stability.

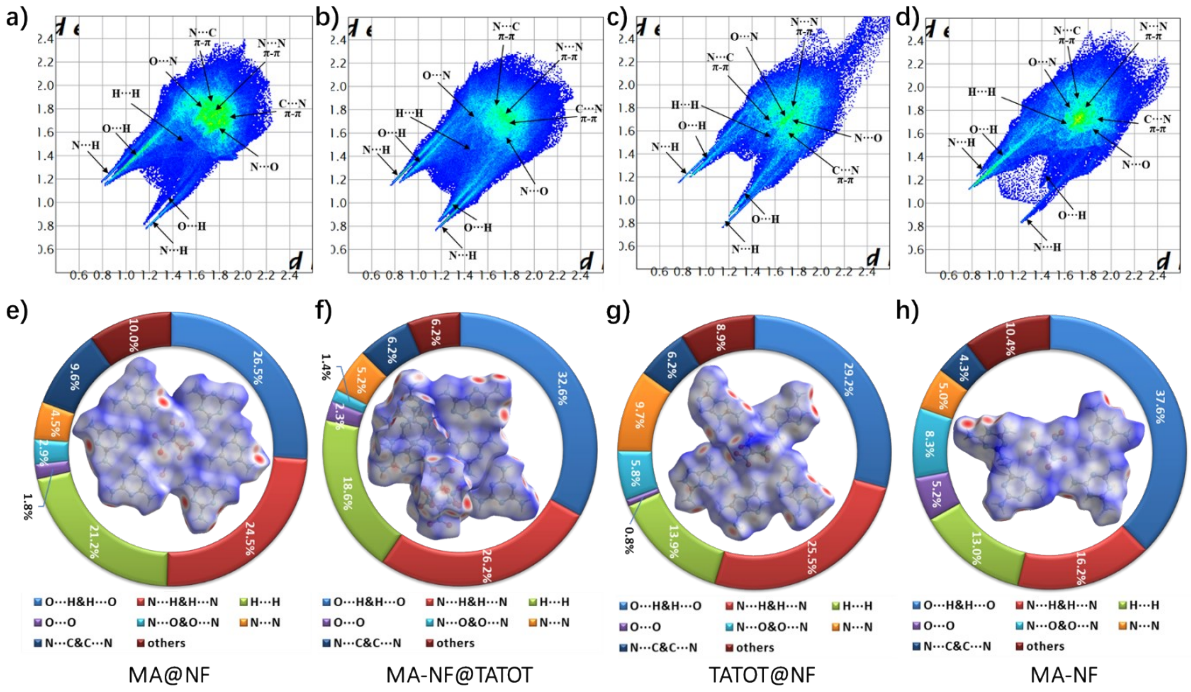

Figure S13. 2D fingerprint calculations and its statistics of interaction types for NF series

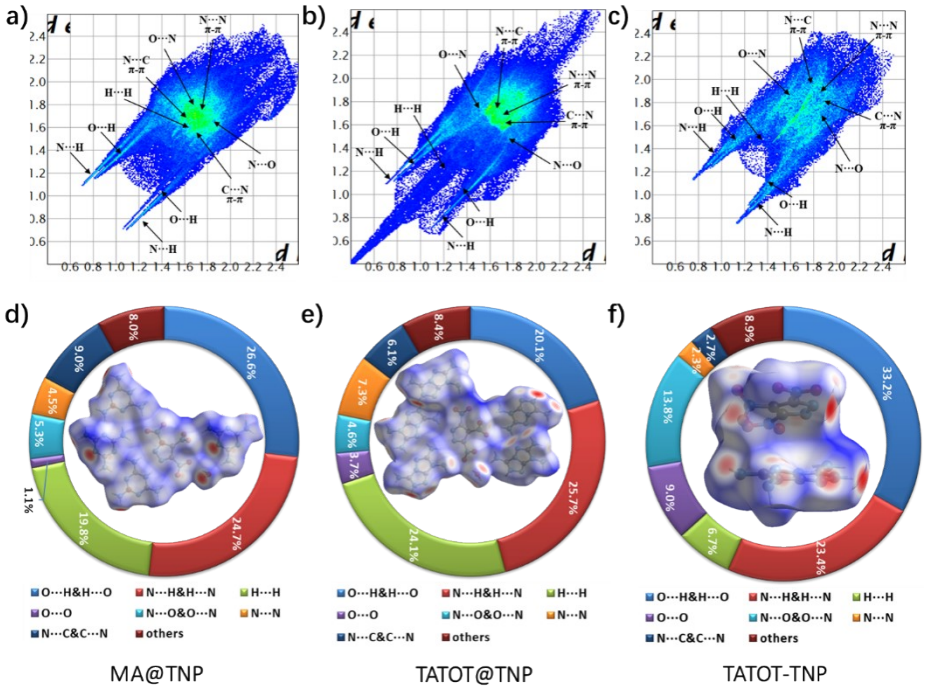

Figure S14. 2D fingerprint calculations and its statistics of interaction types for TNP series

Supplementary section 8: Computational Methods

Theoretical calculations of melamine cation and melamine were performed by using the Gaussian 03 (Revision D.01) suite of scripts.[13] The geometric optimization, frequency analyses and NBO calculations were completed by using the B3LYP functional with the 6-31+G** basis set. Single energy points were calculated at the MP2/6-311++G** level of theory. For all of the compounds, the optimized structures were characterized to be true local energy minima on the potential-energy surface without imaginary frequencies. The gas-phase enthalpies of the building-block molecules were obtained by using the atomization method with the G2 ab initio calculations. For cocrystals, the solid-state heat of formation (HOF, $\Delta_f H°$) was calculated based on a Born–Haber energy cycle[14] with following simplified calculation Equation:

$$\Delta_f H°\text{ (cocrystal, 298K)} = \Delta_f H°\text{(precursor 1, 298K)} + n\Delta_f H°\text{(precursor 2, 298K)} - \Delta H_{sub}\ (n=1 \text{ or } 2)$$

The heat of sublimation can be estimated using the DFT method with the GGARPBE (revised Perdew Burke-Ernzerhof) exchange-correlation functional in Dmol3 program.[15-16]

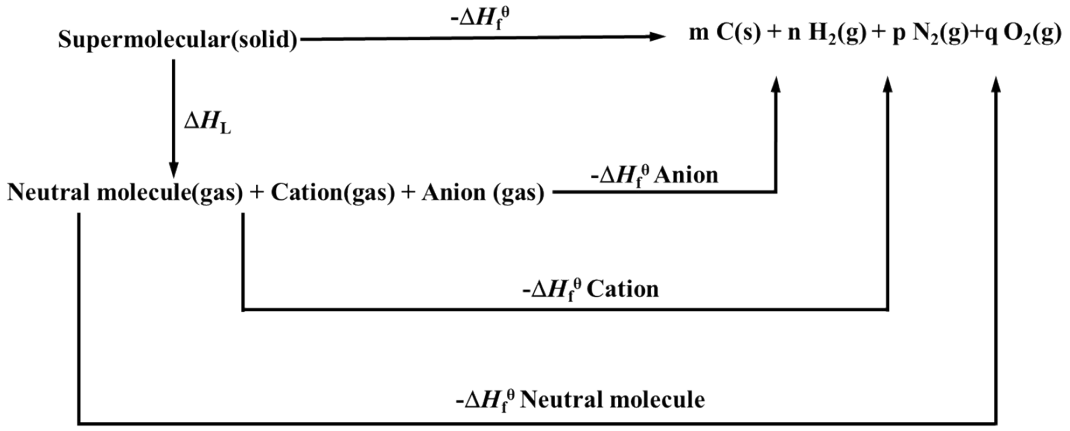

Scheme S1. Born-Haber cycle for the formation of supramolecular.

Table S7. The related heats of formation (HOF) for several species

Species	Heat of formation (kJ mol^{-1}, 298K)
Ma cation	650.8
DN anion	156.2
NF anion	-228.8
TNP anion	-63.1
TATOT cation	1091
Ma	-66.1
TATOT	470.5

References

1. T. M. Klapötke, P. C. Schmid, S. Schnell, J. Stierstorfer, *J. Mater. Chem. A* **2015**, *3*, 2658–2668.

2. J. C. Zhang, Y. A. Feng, R. J. Staples, J. H. Zhang, J. M. Shreeve, *Nat. Comm.* **2021**, *12*, 2146.

3. A. F. Baxter, I. Martin, K. O. Christe, R. Haiges, *J. Am. Chem. Soc.* **2018**, *140*, 15089-15098.

4. P. Yin, J. Zhang, D. A. Parrish, J. M. Shreeve, *J. Mater. Chem. A* **2015,** *3* (16), 8606-8612.

5. E. R. Johnson, S. Keinan, P. Mori-Sánchez, J. Contreras-García, A. J. Cohen, W. T. Yang, *J. Am. Chem. Soc.* **2010**, *132*, 6498-6506.

6. J. H. Zhang, Q. H. Zhang, T. T. Vo, D. A. Parrish, J. M. Shreeve, *J. Am. Chem. Soc.* **2015**, *137*, 1697-1704.

7. S. Grimme, S. Ehrlich, L. Goerigk, *J. Comput. Chem.* **2011**, *32*, 1456-1465.

8. T. Lu, *J. Comput. Chem.* **2012**, *33*, 580-592.

9. W. Humphrey, A. Dalke, K. Schulten, *J. Mol. Graph. Model.* **1996**, *14*, 33-38.

10. S. J. Li, R. P. Bu, R. J. Gou, C. Y. Zhang, *Cryst. Growth Des.* **2021**, *21*, 6619−6634.

11. C. J. Lei, J. Tang, Q. H. Zhang, G. B. Cheng, H. W. Yang, *Org. Lett.* **2023**, *25*, 3487−3491.

12. S. K. Wolff, D. J. Grimwood, J. J. McKinnon, M. J. Turner, D. Jayatilaka, M. A. Spackman, CrystalExplorer, version 3.1; University of Western Australia: Crawley, Australia, **2012**.

13. M. Frisch, Gaussian 03 Rev. E. 01. *http://www. gaussian. com/* (**2004**).

14. V. A. Medvedev, J. Cox, D. D. Wagman, (Hemisphere Publishing Corporation New York, **1989**).

15. B. Delley, *J. Chem. Phys.* **1990**, *92*, 508-517.

16. B. Delley, *J. Chem. Phys.* **2000**, *113*, 7756-7764.